Original Article
Research on mechanical properties of the tongue muscle with a new composite constitutive model validated by experiments

Tong Ou[1], Dayang Wang[2], Chaobo He[2]

[1]Guangdong Architectural Design & Research Institute Co., Ltd., Guangzhou 510000, Guangdong, China; [2]School of Civil Engineering, Guangzhou University, Guangzhou 510006, Guangdong, China

Abstract: The incidence rate of obstructive sleep apnea hypopnea syndrome (OSAHS) is increasing annually, without a clear pathogenesis. It is important for interpreting the pathogenesis of OSAHS to research the mechanical properties of tongue tissues. The goal of this study was to develop a composite constitutive model of the toung to simulate the tension stress-strain and stress relaxation properties of soft muscle tissues. For this purpose, the Mooney-Rivlin (MR) constitutive model representing hyperelastic responses and the Generalized Maxwell (GM) constitutive model were arranged in parallel, representing nonlinear and viscoelastic responses was adopted to create the composite MR-GM constitutive model. Investigations on 30 fresh tongue specimens were then performed under uniaxial tension and stress relaxation experiments to validate the MR-GM constitutive model. A comparative study between the experimental data and the calculated results from the MR-GM constitutive model was conducted on the tension and relaxation properties. Results show that the developed MR-GM constitutive model can well capture the tension stress-strain and stress relaxation performances of the porcine tissues with credible and flexible advantages, which provides an alternative way to represent the mechanical properties of muscle tissues. The porcine specimens show typical hyperelastic, viscoelastic, and anisotropic characteristics.

Keywords: Tongue muscle, constitutive model, mechanical characteristic, tension property, relaxation property

Introduction

According to a relevant survey [1], among American adults, the incidence rate of OSAHS is 4% in males, while it is 2% in females. The incidence rate is on the rise in recent years. However, the pathogenesis of OSAHS is not clear for the time being, and most scholars believe that the obstruction of the pharynx oralis behind the soft palate and the tongue root in the upper airway results in the disease. To reveal the pathogenesis of OSAHS and carry out more in-depth and extensive research, it is necessary to establish a constitutive model of tongue soft tissue as numerical simulation has become an important method in modern medical research [2]. Mechanical modeling has been adopted in many fields, such as clinical medicine, general health, and impact biomechanics [3, 4]. A number of high quality studies in this field have been carried out to capture mechanical properties of various muscles, including the sternocleidomastoideus muscle [3, 5], skeletal muscle [6-8], and the pelvic ring [9], as well as to investigate muscle contraction [10-12]. Among these studies, simulations with the finite element method (FEM) are widely used to predict stress and deformation of muscle tissue. It is well known that the reliability of such simulations depends on the ability to model the complex mechanical behavior of soft tissues and on the identification of associated constitutive data through experiments, such as compression [13, 14], tension [15, 16], and shear experiments [17].

To conduct FEM analysis, the stress-strain relationship is usually the first consideration. The stress-strain can be characterized by hysteresis, sensitivity of strain rate, non-linear elastic, viscoelastic, and permanent strains. Hyperelasticity and viscoelasticity are taken as two

important properties of muscle tissues [18, 19]. Significant effort has been devoted to characterizing the mechanical properties of soft tissues, and various computing models have been developed to describe their mechanical behaviors [20-24]. The constitutive model of simulating human tongue tissue has also been proposed, assuming mostly a hyperelastic material with strain energy approaches [25-27]. However, few studies have suggested a constitutive model based on experimental investigations [28, 29]. Although some constitutive models can capture the gross mechanical behavior of testing specimens, it has been found that the stress-strain relationship and the maximum value have certain differences by comparing these aforementioned experimental studies [30]. For example, the tongue shear modules are 384 Pa in reference [25], 1400 Pa for tongue tissues at "rest" and 8880 Pa for "active" tongue tissues in reference [29], and 2670 Pa in reference [27]. Among these results, the maximum value is more than 20 times the minimum. There might be different reasons for these discrepancies, such as specimen selection, preparation method, realization of the experiments, and evaluation or interpretation of the results. Therefore, it will be important and necessary to conduct further studies to improve the quality of research in this field.

This study aims to propose a composed constitutive model, namely the MR-GM constitutive model, which is expected to represent a full viscoelastic and hyperelastic characterization of tongue muscle tissues. This constitutive model will likely be suitable for the desired characterization because it can accurately capture the stress-strain behaviors of both the toe stage and linear stage of muscle tissues [18, 31], and it enables fitting precision to be closer to reality. Additionally, the proposed constitutive model can capture the stress relaxation behavior of muscle tissues in different initial loading stresses using unified material parameters. To achieve these purposes, 30 experimental specimens are subjected to uniaxial tension and stress relaxation testing. Due to the unavailability of tongue samples, pig tongue is proposed to be used in this study as the porcine muscles are anatomically and physiologically similar to human muscles [32]. All experi-

mental specimens are from five-month-old male pigs. The experimental results are then used to validate the proposed constitutive model via systematic comparison between experimental and calculated tension and relaxation data. Results of this study are helpful to further investigate the pathogenesis of OSAHS, especially adopting the method of numerical simulation.

Material and methods

Specimen preparation

Tongue material of four male pigs with an average weight of 65 kg was obtained after animal sacrifice. This experiment was approved by the China Laboratory Animal-Guideline for Ethical Review of Animal Welfare. Experimental specimens with the required dimensions were cut from selected tongues and then immediately immersed in a saline solution at 4°C to keep them fresh and prevent degradation [38]. Cutting specimens with ideal size and fixed fiber direction is difficult due to the mobility of freshly harvested muscles tissues and the limited availability of the tissues in the correct fiber orientation. In this study, the ratios of the length to width and the width to thickness of the tissue specimens are designed to be five and three, respectively, which are considered to be acceptable and effective experimental dimensions [39]. In total, 30 specimens of tongue tip, tongue center, and tongue root, were prepared: 18 specimens for uniaxial tension experiments and 12 specimens for stress relaxation experiments. Details of the 30 specimens are given in **Table 1**.

Experimental protocol

To minimize the influence of rigor mortis on the results, experiments were conducted within 2 h after sacrifice [40]. BOSE Electro Force 3220 was adopted as the testing equipment. Force transducers, with a bearing capacity of 50 N, accuracy of ± 2.5%, response time of less than 5 μs, and drift of < 3% per logarithmic timescale, were installed to record experimental data. The upper extremity was firstly fixed in the upper jaw. Then, the specimen was submitted to gravity to reach a vertical position. Finally, the lower extremity was fixed in the lower jaw.

Table 1. Specimen design of tongue muscle tissues

Specimens of uniaxial tension experiment							Specimens of stress relaxation experiment				
Tissue direction	Tongue tip		Tongue center		Tongue root		Description	Transverse		Longitudinal	
	No.	L×W×T	No.	L×W×T	No.	L×W×T		No.	ILD	No.	ILD
Transverse	TT1	50×9×3	TC1	50×9×3	TR1	50×9×3	Tongue center	RT1	5.2	RL1	5.2
	TT2	50×10×4	TC2	50×10×4	TR2	50×10×4		RT2	5.8	RL2	5.8
	TT3	50×11×5	TC3	50×11×5	TR3	50×11×5		RT3	6.3	RL3	6.3
Longitudinal	TT4	50×9×3	TC4	50×9×3	TR4	50×9×3	L×W×T: 50×9×3	RT4	7.0	RL4	7.0
	TT5	50×10×4	TC5	50×10×4	TR5	50×10×4		RT5	7.4	RL5	7.4
	TT6	50×11×5	TC6	50×11×5	TR6	50×11×5		RT6	8.5	RL6	8.5

Note: L×W×T means length × width × thickness (mm). ILD means initial loading displacement (mm). TT, TC, TR, RT and RL mean tongue tip, tongue center, tongue root, transverse and longitudinal specimens.
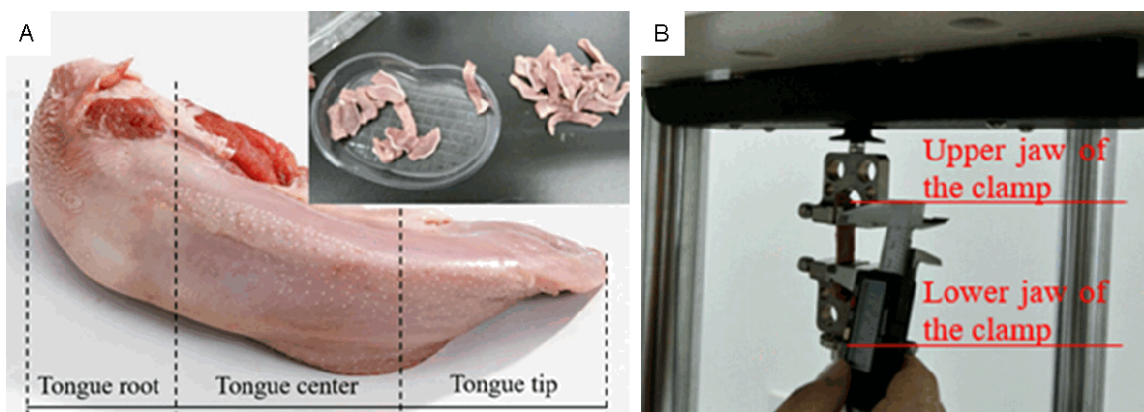
Figure 1. Test specimen: (A) specimen preparation and (B) specimen setup.

To avoid slippage between the tissue and the clamps, each specimen was attached to sandpaper tabs using cyanoacrylate cement before being placed in the experimental equipment [5]. Specimen preparation and experimental setup are described in **Figure 1**. This study was approved by the ethics committee of the author's university.

In the uniaxial tension test, a testing velocity of 0.2 L/100 mm min^{-1} was ensured (L is the initial specimen length and 0.2 is the deformation rate) [41]. In the stress relaxation test, the duration of each measurement and the pause between subsequent preconditioning indentations at the same site are set to be 30 s [42], which require that all measurements are completed early enough before rigor mortis occurs. Before the tests begin, a certain loading is imposed to obtain the required initial geometrical parameters. Saline spray is used to maintain the specimen moistness, and the experiments were conducted in the open air with

room temperature of 25°C. To reach the required temperature, the tissue specimens were arranged in the air for a few minutes to equilibrate with the temperature before tests. Summary statistics were calculated using a one-way ANOVA with significance set at $P < 0.05$ [17].

MR-GM constitutive method

Tongue muscle shows complex nonlinear, time dependent, viscoelastic, and anisotropic characteristics. The passive response of the muscle tissues is generally hyperelastic and viscoelastic. The choice of an appropriate constitutive law is usually a key point of modeling the hyperelastic materials. Phenomenological models involving strain-energy density functions, which are represented by the neo-Hookean model, Mooney-Rivlin model, and Ogden model normally, are frequently adopted as their good performance of fitting various phenomena including the onset of instabilities

[33]. To represent the stress relaxation behavior of viscoelastic materials more rigorously, the Generalized Maxwell model, namely one more springs added in parallel with the other Maxwell elements, is usually used [34]. Thus, in this study, a composed MR-GM constitutive model was proposed, with the MR model representing the hyperelastic responses and the GM model arranged in parallel representing the nonlinear and viscoelastic responses. The stress σ and strain ε of the MR-GM model can then be expressed:

$$\begin{cases} \sigma = \sigma_H + \sigma_{VE} \\ \varepsilon = \varepsilon_H = \varepsilon_{VE} \end{cases} \tag{1}$$

where σ_H and ε_H are the stress and strain of the MR model, and σ_{VE} and ε_{VE} are the stress and strain of the GM model.

For a conservative system, the elastic Cauchy stresses are derived from the strain-energy density function per unit of undeformed volume W, which can be written in terms of the principle invariants I_1, I_2, and I_3 of the right Cauchy-Green tensor. Soft materials exhibit small volume changes, so incompressibility is usually assumed for simplicity [35]. Therefore, $I_3 = 1$ is adopted in this study assuming tongue tissues are incompressible. The Mooney-Rivlin strain-energy density function can be expressed as the following equation:

$$W = C_1 (I_1 - 3) + C_2 (I_2 - 3) \tag{2}$$

where C_1 and C_2 are the material constants and can be determined by experimental data. Based on the relationship between the Kirchhoff stress tensor t_{ij} and the Green strain tensor γ_{ij}, the following equation can be obtained [36]:

$$t_{ij} = \frac{\partial W}{\partial \gamma_{ij}} = \frac{\partial W}{\partial I_1}\frac{\partial I_1}{\partial \gamma_{ij}} + \frac{\partial W}{\partial I_2}\frac{\partial I_2}{\partial \gamma_{ij}} + \frac{\partial W}{\partial I_3}\frac{\partial I_3}{\partial \gamma_{ij}} \tag{3}$$

Considering equation of $\lambda_i = 1+\gamma_i$, relationship between the principal stress t_i and the principal stretch λ_i is as the following considering [36]:

$$t_i = \lambda_i \frac{\partial W}{\partial \lambda_i} + P = 2\left(\lambda_i^2 \frac{\partial W}{\partial I_1} + \frac{1}{\lambda_i^2}\frac{\partial W}{\partial I_2}\right) + P \tag{4}$$

where P is an unknown hydrostatic pressure, representing incompressible performance and stress insensitivity of hyperelastic materials. The differences between the three principal stresses can be expressed as:

$$t_1 - t_2 = 2\left(\lambda_1^2 - \lambda_2^2\right)\left(\frac{\partial W}{\partial I_1} + \lambda_3^2 \frac{\partial W}{\partial I_2}\right) \tag{5a}$$

$$t_2 - t_3 = 2\left(\lambda_2^2 - \lambda_3^2\right)\left(\frac{\partial W}{\partial I_1} + \lambda_1^2 \frac{\partial W}{\partial I_2}\right) \tag{5b}$$

$$t_3 - t_1 = 2\left(\lambda_3^2 - \lambda_2^2\right)\left(\frac{\partial W}{\partial I_1} + \lambda_2^2 \frac{\partial W}{\partial I_1}\right) \tag{5c}$$

If considering only the uniaxial tension state, namely $t_2 = t_3 = 0$, then we have $\lambda_2^2 = \lambda_3^2 = 1/\lambda_1 = 1/\lambda$. In this state, the principle invariants can be expressed:

$$I_1 = \lambda_1^2 + \lambda_2^2 + \lambda_3^2 = \lambda^2 + 2/\lambda \tag{6a}$$

$$I_2 = \lambda_1^2\lambda_2^2 + \lambda_2^2\lambda_3^2 + \lambda_3^2\lambda_1^2 = 2\lambda + 1/\lambda^2 \tag{6a}$$

$$I_3 = \lambda_1^2\lambda_2^2\lambda_3^2 = 1 \tag{6a}$$

Combining Equations (4)-(6), The principal stress t_i can be deduced:

$$t_i = 2\left(\lambda^2 - \frac{1}{\lambda}\right)\left(C_1 + \frac{1}{\lambda}C_2\right) \tag{7}$$

where t_1 is the true stress and can be transferred to be engineering stress σ ($\sigma = t/\lambda$). Finally, the stress-strain equation of the MR constitutive model can be expressed as:

$$\sigma_H = 2\left(\lambda - \frac{1}{\lambda^2}\right)\left(C_1 + \frac{1}{\lambda}C_2\right) \tag{8}$$

Equation (8) can also be expressed as a function of the strain ε:

$$\sigma_H = 2C_1\left[1 + \varepsilon - \frac{1}{(1+\varepsilon)^2}\right] + 2C_2\left[1 - \frac{1}{(1+\varepsilon)^3}\right] \tag{9}$$

For the GM constitutive model, the stress σ_{VE} is given by:

$$\sigma_{VE} = E_0\varepsilon + \sum_{i=1}^{n} E_i\varepsilon_{Ei} \tag{10}$$

where E_i is the modulus of the spring in the ith Maxwell element. In the ith Maxwell element, the stress of the spring is equal to the stress of
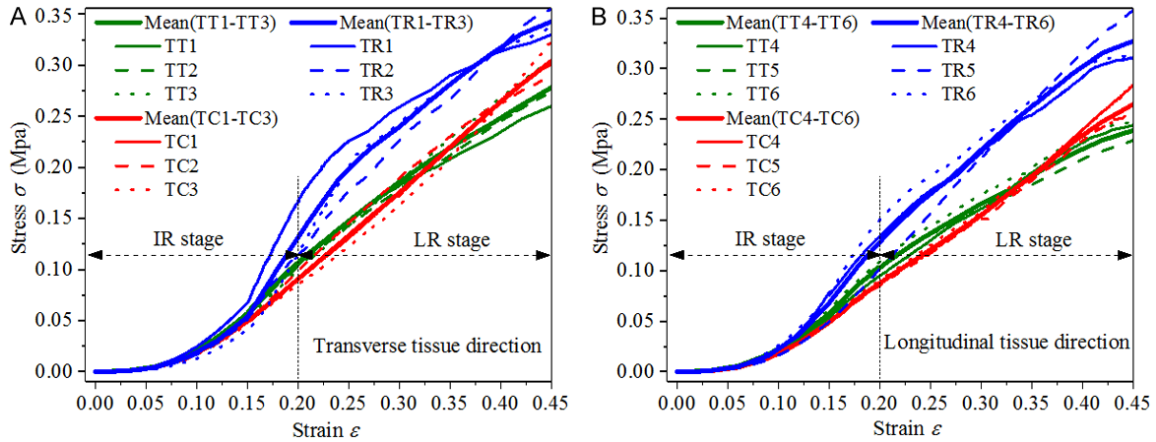
Figure 2. Stress-strain curves: (A) Transverse direction and (B) longitudinal direction.

the dashpot, namely $\sigma_{Ei} = \sigma_{vi}$. Equation (10) can also be written as:

$$\sigma_{VE} = E_0\varepsilon + \sum_{i=1}^{n} \eta_i \frac{d\varepsilon_{Vi}}{dt} \quad (11)$$

Therefore, the total stress of the MR-GM constitutive model is:

$$\sigma = \sigma_H + \sigma_{VE} = 2C_1\left[1 + \varepsilon - \frac{1}{(1+\varepsilon)^2}\right] + \\ 2C_2\left[1 - \frac{1}{(1+\varepsilon)^3}\right] + E_0\varepsilon + \sum_{i=1}^{n} \eta_i \frac{d\varepsilon_{Vi}}{dt} \quad (12)$$

In the process of stress relaxation, the tissues are firstly loaded to a predesigned tension state, and then loading is stopped to observe the stress relaxation. It is well known that the hyperelastic characteristics of soft tissues cannot reflect relaxation, which can be explained by its relaxation modulus $E_H(t)$:

$$E_H(t) = \frac{d\sigma_H}{d\varepsilon} = 2C_{10} + 4C_{10}\frac{1}{(1+\varepsilon)^3} + 6C_{01}\frac{1}{(1+\varepsilon)^4} \quad (13)$$

The relaxation modulus $E_H(t)$ is a constant during the relaxation process, and the stress will remain unchangeable over time for the hyperelastic model. Consequently, relaxation for the MR-GM model is mainly dominated by the GM model. The relaxation modulus $E_{VR}(t)$ of the GM model is represented as:

$$E_{VR}(t) = E_0 + \sum_{i=1}^{n} E_i e^{(-t/\tau_R)} \quad (14)$$

where E_0 represents the stiffness at initial time [37]. The stress response with time dur-

ing relaxation for the GM model can be obtained:

$$\sigma_{VE} = \int E(t)d\varepsilon = E_0\varepsilon + \left(\sum_{i=1}^{n} E_i\varepsilon + b\right)e^{(-t/\tau_R)} \quad (15)$$

Then, the total stress of the MR-GM constitutive model is as follows:

$$\sigma = 2C_1\left[1 + \varepsilon - \frac{1}{(1+\varepsilon)^2}\right] + 2C_2\left[1 - \frac{1}{(1+\varepsilon)^3}\right] + \\ E_0\varepsilon + \left(\sum_{i=1}^{n} E_i\varepsilon + b\right)e^{(-t/\tau_R)} \quad (16)$$

In Equations (12) and (16), C_1, C_2, E, η, and b are all material constants and can be determined by experimental data.

Results

Results of tension experiment

The stress-strain relationships of the 18 specimens are shown in **Figure 2**. It can be observed that all stresses appear to increase with increasing strain. At the same strain, the stress of the tongue root is the largest, followed by the tongue center, and finally the tongue tip, especially at higher strains. As for the same part of the tongue tissues, the stresses of transverse directions are larger than those of longitudinal directions, indicating that there is a certain anisotropic characteristic for the muscle tissues, and this characteristic becomes more significant with growing strains. Generally speaking, the smaller the stress, the stronger the viscoelastic characteristics of muscle tissues under the same strain. Therefore, it can
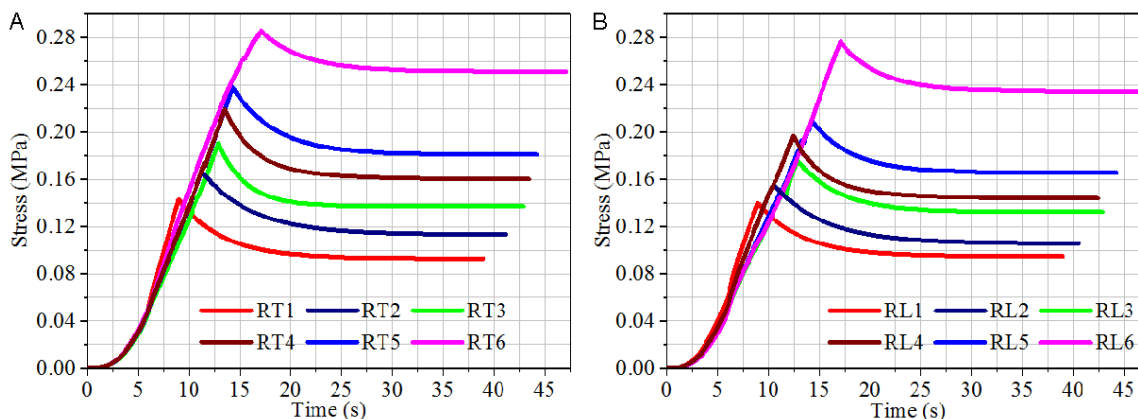
Figure 3. Stress relaxation behavior: (A) transverse and (B) longitudinal specimens.

be concluded that the viscoelastic characteristics of the tongue tip tissues are the strongest, followed by the tongue center tissues, and finally the tongue root tissues under the condition of the same tissue direction. The viscoelastic characteristics of the longitudinal tissues are stronger than those of the transverse tissues under the condition of the same muscle part.

Furthermore, two different change stages, namely index rising (IR) stage and linear rising (LR) stage, can be determined. In the IR stage, stress increases rapidly with power exponent greater than one, whereas in the LR stage, stress increases linearly with strain. This phenomenon can also be found by Fung [18]. Based on the experimental data shown in **Figure 3**, the separation between the IR and LR stages can be defined as the strain point of ε = 0.2, meaning that the stress-strain relationship is in the IR stage if the strain satisfies $\varepsilon \in [0, 0.2]$ and in the LR stage if $\varepsilon \in [0.2, 0.45]$.

Results of relaxation experiment

Figure 3 shows the relationship between stress and loading time of the 12 specimens. All specimens exhibit relaxation effect once they are loaded into the defined initial status and then offloaded. The relaxation effect is significant at the beginning, with the phenomenon of great stress reduction. After that, the reduction degree starts to decrease gradually, and finally no reduction is detected, indicating the completion of stress relaxation. It is worth mentioning that the relaxation effect shows a nearly linear decreasing with increasing initial stress for tissues of the same part with the same dimen-

sion. The final stress relaxation ratio, equaling to $(\sigma_0 - \sigma_F)/\sigma_0 \times 100\%$, where σ_0 and σ_F are the initial and the final stresses, for the specimens of RL1, RL2, RL3, RL4, RL5, and RL6 are 30.8%, 28.5%, 24.3%, 22.4%, 20.6%, and 14.6%, where the corresponding initial stresses are 0.143 MPa, 0.156 MPa, 0.176 MPa, 0.197 MPa, 0.21 MPa, and 0.276 MPa, respectively. The initial stress is a decisive factor influencing the final stress for muscle tissues, indicating that the initial strain should be determined accurately to obtain a reliable stress relaxation effect of the tongue specimens.

Discussion

Fitting of the experimental data is performed with an implementation of the Levenberg-Marquardt minimization algorithm using two evaluation indexes: the determination coefficient R^2 and the normalized mean square root error κ [43].

Discussion on tension property

MR constitutive model: The material constants of C_1 and C_2 should be determined to perform MR evaluation, which is finished by linear-regression analysis of the experimental datagram between $1/\lambda$ and $\sigma_H/[2(\lambda-1/\lambda^2)]$. As discussed in Section 3, there are two change stages for the tension stress-strain curves, the IR stage and the LR stage, indicating that the two constants can be determined by different linear-regression equations with different experimental data. Thus, three fitting linear equations, namely LE_{IR}, LE_{LR}, and LE_{ALL}, are adopted. The linear equation LE_{IRS} is from the
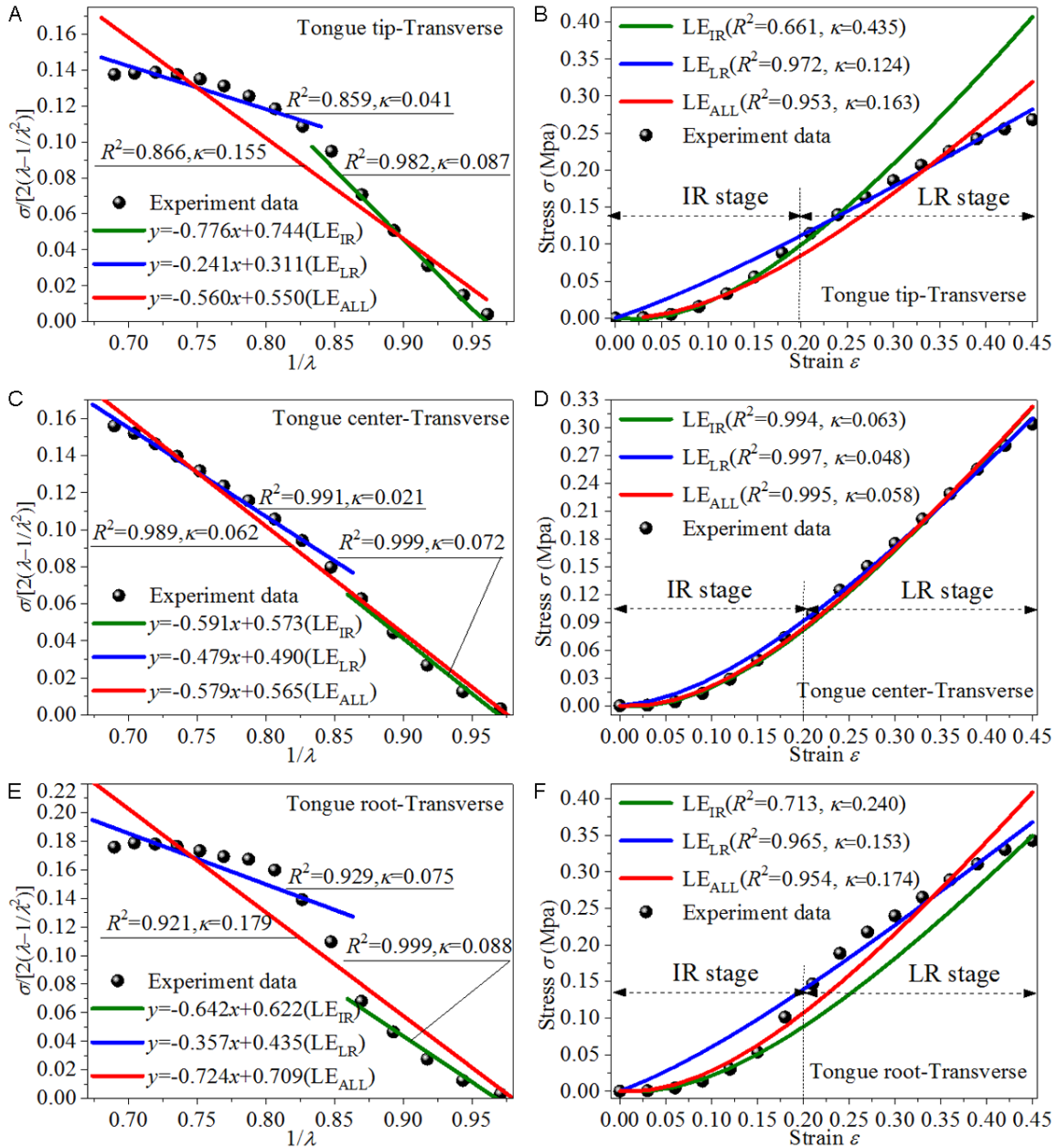
Figure 4. Fitting based on the MR model. (A) Definition of the material constants of the transverse tongue tip muscle. (B) Experimental versus analytical stress-strain relationships based on the material constants obtained in (A). (C) Definition of the material constants of the transverse tongue center muscle. (D) Experimental versus analytical stress-strain relationships based on the material constants obtained in (C). (E) Definition of the material constants of the transverse tongue root muscle. (F) Experimental versus analytical stress-strain relationships based on the material constants obtained in (E).

fitting with experimental data of the IR stage with $\varepsilon \in [0, 0.2]$. The linear equation LE_{LRS} is from the fitting of the LR stage with $\varepsilon \in [0.2, 0.45]$. The linear equation LE_{ALL} is from the fitting with all experimental data. The material constants of C_1 and C_2 are determined and shown in **Figure 4A**, **4C** and **4E**.

Although the material constants of the MR model can be determined with two-stage fitting of IR and LR, these material constants can only ensure good agreement for the corresponding IR stage or LR stage. For instance, in **Figure 4B**, good fitting between the fitting and experimental data can be found in the IR stage if using

Table 2. Material constants of the MR-GM model determined by fitting with experiment

Case	C_1	C_2	E_0	η_1	η_2	R^2	κ
TT1-3	0.5624	-0.5837	0.045	0.037	0.026	0.9710	0.1274
TC1-3	0.5624	-0.5807	0.045	0.035	0.026	0.9952	0.0567
TR1-3	0.6724	-0.6737	0.4	0.03	0.026	0.9853	0.0968
TT4-6	0.5408	-0.5582	0.048	0.035	0.026	0.9695	0.1251
TC4-6	0.5664	-0.5892	0.043	0.035	0.025	0.9912	0.0743
TR4-6	0.5329	-0.5125	0.047	0.028	0.02	0.9834	0.0975

material constants from LE_{IR}, but in the LR stage, the fitting is poor with significant discretization to the experiment data. This phenomenon can also be found in **Figure 4F**. Consequently, if the material constants from LE_{ALL} are adopted, the fitting curves seem to exhibit a certain improvement without significant discretization with the experiment data, that is, the fitting curves can reflect the stress-strain relationships of both the IR and LR stages to some extent. However, the fitting results are still undesirable. Although the coefficients of determination R^2 are obtained to be close to one, the normalized mean square root errors κ are somewhat far from the ideal value of zero. As shown in **Figure 4B**, the fitting errors of (R^2, κ) based on determined material constants of LE_{ALL} are (0.953, 0.163).

Furthermore, it can be detected that the best fitting can be achieved only when the relationship between $1/\lambda$ and $\sigma/[2(\lambda-1/\lambda^2)]$ is linear. As shown in **Figure 4D**, the fitting errors (R^2, κ) based on the determined material constants of LE_{IRS}, LE_{LRS}, and LE_{ALL} are (0.994, 0.063), (0.997, 0.048), and (0.995, 0.058), respectively. In other words, the MR constitutive model can credibly reflect the stress-strain relationship of soft tissues in the above condition with perfect fitting errors of R^2 close to one and κ close to zero. Otherwise, there are some difficulties or imperfections in fitting the experimental data with the MR model regardless of the methods used to determine the material constants. Therefore, it can be concluded that the MR constitutive model has certain limitations in fitting the hyperelastic stress-strain of soft tissues since it can guarantee a perfect fitting only in the condition of a linear relationship between $1/\lambda$ and $\sigma/[2(\lambda-1/\lambda^2)]$.

MR-GM constitutive model: The material constants of the MR-GM model describing the mean stress-strain of the specimens are fitted. **Table 2** shows the fitted material constants of the MR-GM model as well as the fitting errors (R^2, κ). It can be found that the MR-GM model can well describe the tension stress-strain relationship with acceptable fitting errors, especially for the tongue center and tongue root specimens. For example, the fitting errors ($R^2$, κ) are (0.9952, 0.0567) for transverse tongue center specimens and (0.9853, 0.0968) for transverse tongue root specimens. For the tongue tip specimens, the normalized mean square roots are somewhat higher, at 0.1274 and 0.1251 for transverse and longitudinal specimens, but the corresponding coefficients of determination are close to one, at 0.971 and 0.9834, respectively. The reason for this phenomenon may be caused by stronger viscoelastic characteristics of the tongue tip specimens relative to the tongue center and root specimens, indicating that more Maxwell elements will be needed to capture the tension stress-strain relationship of muscle tissues with stronger viscoelasticity.

Figure 5 shows a comparison of the stress-strain among experimental data and theoretical methods of MR-GM and MR constitutive models. The material constants of the MR constitutive model are from the fitting equation of LE_{ALL}. It can be found that the fittings of the MR-GM model to the experimental data are better than those of the MR model for all the specimens of tongue tip, center, and root, meaning good agreement for the MR-GM model. Values of R^2 and κ calculated by the MR-GM model are much closer to the ideal values of one and zero, respectively, than those of the MR model. For example, the fitting errors (R^2, κ) for the MR-GM and MR constitutive models are (0.971, 0.1274) and (0.953, 0.163), respectively, in **Figure 5A**, and (0.9834, 0.0975) and (0.967, 0.141), respectively, in **Figure 5F**. So, it can be obtained that MR-GM model appears to be more reliable of reflecting the mechanical behaviors of the muscle tissues compared to the MR model.

It can be achieved that the hyperelastic behavior of the tongue tissues can be captured by the MR-GM model, especially in the IR stage. As shown in **Figure 5**, the stress-strain relation-
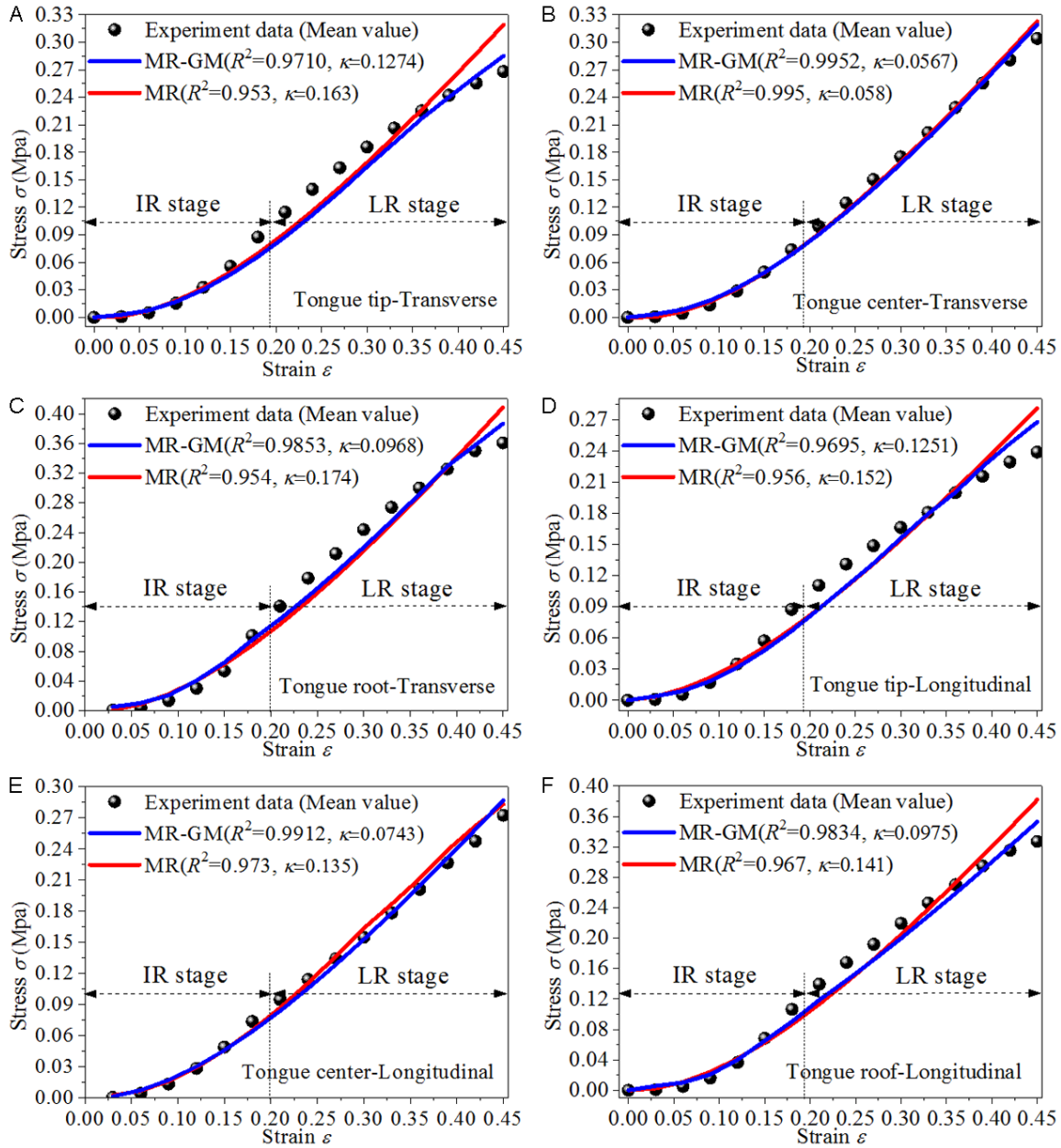
Figure 5. Fitting comparisons among experiment data and theoretical methods: (A) Tongue tip-Transverse, (B) Tongue center-Transverse, (C) Tongue root-Transverse, (D) Tongue tip-Longitudinal, (E) Tongue center-Longitudinal, and (F) Tongue roof-Longitudinal.

ships of the IR stage appear coincidence between the MR-GM model and the experiment data, no matter in different parts (tongue tip, center and root) or in different directions (Transverse and longitudinal). As for the LR stage, it can be found that the coincidence of the transverse and longitudinal tongue center specimens appears the best (**Figure 5B**, **5E**), followed by the transverse and longitudinal tongue root specimens (**Figure 5C**, **5F**), and the

last the transverse and longitudinal tongue tip specimens (**Figure 5A**, **5D**). Although there are some errors between the MR-GM model and the experiment data because of human operation in experiment and simplified treatment in constitutive model, the fitting of the MR-GM model to the experiment data appear acceptable and represent the hyperelastic characteristics well. Thus, it can be determined that the MR-GM model has excellent capacity for cap-

Table 3. Material constants determined by MR-GM constitutive model with relaxation experimental data

Specimen	C_1	C_2	E_0	E_1	E_2	τ_R	R^2	κ
RT1	0.5753	-0.6328	0.02	0.055	0.015	4.2	0.9947	0.0094
RT2	0.5753	-0.6328	0.02	0.055	0.015	4.2	0.9850	0.0142
RT3	0.5753	-0.6328	0.02	0.055	0.015	2.5	0.9946	0.0064
RT4	0.5753	-0.6328	0.02	0.055	0.015	3.3	0.9986	0.0031
RT5	0.5753	-0.6328	0.02	0.055	0.015	4.2	0.9978	0.0036
RT6	0.5753	-0.6328	0.02	0.055	0.015	4.2	0.9992	0.0010
RL1	0.5753	-0.6328	0.02	0.055	0.015	4.0	0.9974	0.0058
RL2	0.5753	-0.6328	0.02	0.055	0.015	4.5	0.9959	0.0074
RL3	0.5753	-0.6328	0.02	0.055	0.015	4.0	0.9975	0.0041
RL4	0.5753	-0.6328	0.02	0.055	0.015	3.5	0.9973	0.0043
RL5	0.5753	-0.6328	0.02	0.055	0.015	4.0	0.9992	0.0018
RL6	0.5753	-0.6328	0.02	0.055	0.015	4.0	0.9998	0.0006

turing the hyperelastic behavior of the tongue tissues.

Discussion on relaxation property

The MR-GM constitutive model is adopted in this section to fit the stress relaxation properties of the tongue muscle specimens and the corresponding material constants. The fitting constants are shown in **Table 3**. It is observed that the stress relaxation characteristics of the 12 specimens can be captured with a high degree of consistency with the proposed MR-GM constitutive model. The fitting errors (R^2, κ) of both the transverse and longitudinal specimen tissues are basically equal to the target optimal values (1, 0). For example, as shown in **Table 3**, the R^2 values of specimens RT1, RT2, RT3, RT4, RT5, and RT6 are 0.9947, 0.985, 0.9946, 0.9986, 0.9978, and 0.9992, respectively, and the corresponding κ values are 0.0094, 0.0142, 0.0064, 0.0031, 0.0036, and 0.0010, respectively. Therefore, it can be further determined that the MR-GM model has excellent capacity of capturing the stress relaxation properties of the tongue muscles with reasonable fitting errors.

As shown in **Figures 6** and **7**, the MR-GM constitutive model can fit all the relaxation properties of relaxation stress and relaxation function of the 12 tongue specimens with different initial loading stresses using a group of unified material constants C_1, C_2, E_0, E_1, and E_2 (**Table 3**), which can be determined from the experimental data of any one of the experimental speci-

mens. Then, based on the unified material constants, the stress relaxation of the tongue specimens can be captured by computing the initial loading strain ε and the material relaxation time constant τ_R. Therefore, the MR-GM constitutive model is more flexible and simple for fitting the stress relaxation properties of tongue tissues, and the corresponding results appear to be more reliable. The stress relaxation curves shown in **Figures 6** and **7** reveal good agreement between the measured data and the theoretical calculations of the MR-GM model with the unified material constants, indicating the proposed MR-GM model has an excellent capacity for capturing both the hyperelastic tension behavior and the viscoelastic stress relaxation behavior of tongue tissues.

Conclusions

A composed MR-GM constitutive model based on MR and GM constitutive models is developed and validated by experiment data of mechanical performance of 30 porcine tongue muscle tissues. The validated MR-GM model and corresponding results illuminate new ways of investing the pathogenesis of OSAHS by using numerical methods, such as 3D patient-specific numerical modeling and parameter influence analysis. The main conclusions are as follows:

1. The stress-strain and relaxation behaviors of the porcine specimens can be well fitted by the developed MR-GM constitutive model. MR-GM constitutive model is not only better for capturing the tension hyperelastic property than that of MR constitutive model, but also more flexible and reliable for capturing the relaxation viscoelastic performance with unified material constants, which provides an alternative way of representing the tension and relaxation properties of muscle tissues.

2. The tension stress of the specimens all appears increasing with increasing loading strain. The stress-strain relationship can be divided into two stages with the separation
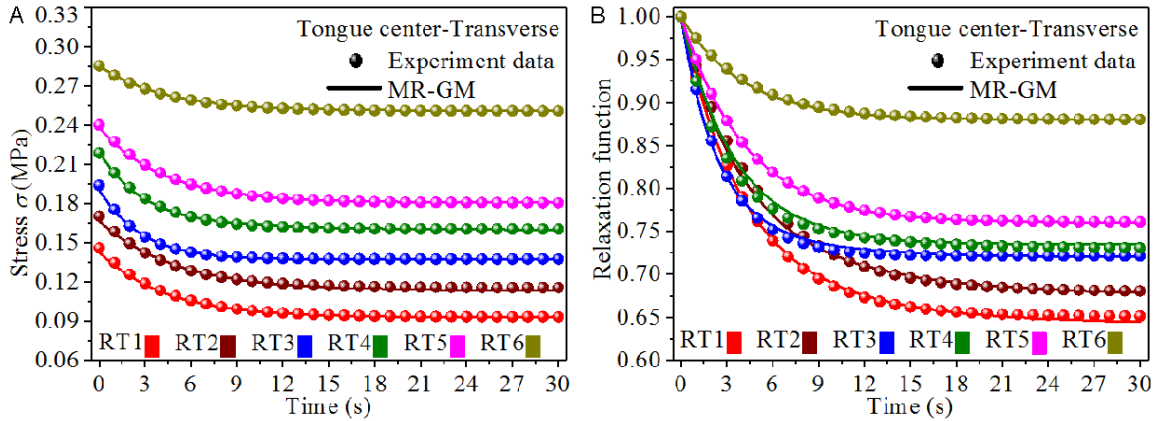
Figure 6. Comparison curves of the transverse specimens: (A) Stress relaxation and (B) Relaxation function.
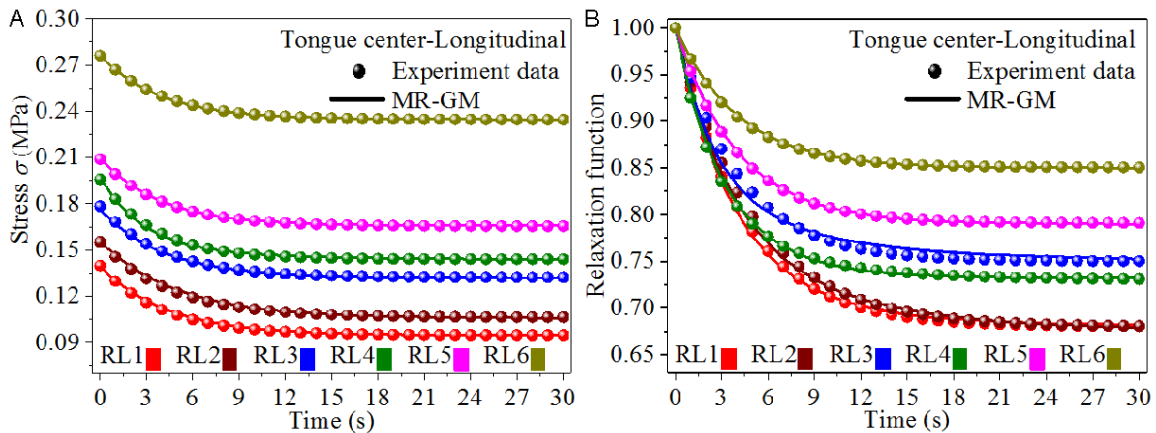
Figure 7. Comparison curves of the longitudinal specimens: (A) Stress relaxation and (B) Relaxation function.

point at $\varepsilon = 0.2$, namely IR stage and LR stage. In the same strain, mean stresses of the tongue root specimens are the largest, then the tongue center specimen and finally the tongue tip specimen, especially for the larger strains.

3. Significant stress relaxation effects can be obtained for all specimens, which show swift stress reduction at the beginning and then gentle reduction after that. The initial loading stress play a key role of affecting the relaxation effect, and the greater the loading stress, the smaller the final stress relaxation ratio. A linear relationship between the initial loading stress and the final stress relaxation ratio can be concluded.

Disclosure of conflict of interest

None.

Address correspondence to: Dayang Wang, School of Civil Engineering of Guangzhou University, Executive East Building No. 513, West Waihuan Road 230, Panyu District, Guangzhou 510006, Guangdong, China. E-mail: wadaya2015@gzhu.edu.cn

References

[1] Young T, Palta M, Dempsey J, Skatrud J and Badr S. The occurrence of sleep-disordered breathing among middle-aged adults. N Eng J Med 1993; 328: 1230-1235.

[2] Liu HL, Prot VE and Skallerud BH. 3D patient-specific numerical modeling of the soft palate considering adhesion from the tongue. J Biomech 2018; 77: 107-114.

[3] Spyrou LA, Agoras M and Danas K. A homogenization model of the Voigt type for skeletal muscle. J Theor Biol 2017; 414: 50-61.

[4] Gefen A, Kottner J and Santamaria N. Clinical and biomechanical perspectives on pressure injury prevention research: the case of prophylactic dressings. Clin Biomech (Bristol, Avon) 2016; 38: 29-34.

[5] Gras LL, Mitton D, Viot P and Laporte S. Hyper-elastic properties of the human sternocleido-mastoideus muscle in tension. J Mech Behav Biomed 2012; 60: 131-140.

[6] Martins JAC, Pires EB, Salvado R and Dinis PB. A numerical model of passive and active behavior of skeletal muscles. Comput Method Appl M 1998; 151: 419-433.

[7] Eby SF, Cloud BA, Brandenburg JE, Giambini H, Song PF, Chen SG, Lebrasseur NK and An KN. Shear wave elastography of passive skeletal muscle stiffness: influences of sex and age throughout adulthood. Clin Biomech (Bristol, Avon) 2015; 30: 22-27.

[8] Neto MF and Figueiredo ML. Skeletal muscle signal peptide optimization for enhancing propeptide or cytokine secretion. J Theor Biol 2016; 409: 11-17.

[9] Leumann A, Fortuna R, Leonard T, Valderrabano V and Herzog W. Dynamic in-vivo force transfer in the lapine knee loaded by quadriceps muscle contraction. Clin Biomech (Bristol, Avon) 2013; 28: 199-204.

[10] Tan T and De Vita R. A structural constitutive model for smooth muscle contraction in biological tissues. J Mech Med Biol 2015; 22: 791-796.

[11] Kim YH, Loeb GE, Peck RA, Singh J, Deshpande S, Baker LL and Bryant JT. A failure analysis of intramuscular rigid implants for muscle contractions. J Mech Phys Solids 2008; 94: 490-503.

[12] De Vita R, Grange R, Nardinocchi P and Teresi L. Mathematical model for isometric and isotonic muscle contractions. J Theor Biol 2017; 425: 1-10.

[13] Kak DW, Anita AR, Nizlan NM, Normala I, Abdul Jalil NA and Wong SV. Compression of neck muscle electromyography activity in response to external force betaeen static and dynamic loading. J Mech Med Biol 2019; 19: 1850034.

[14] Van Loocke M, Lyons CG and Simms CK. A validated model of passive muscle in compression. J Biomech 2006; 39: 2999-3009.

[15] Wan C, Hao ZX and Wen SZ. A comparison of material characterizations in frequently used constitutive models of ligaments. Int J Nnumer Meth Bio 2014; 30: 605-615.

[16] Noonan TJ, Best TM, Seaber AV and Garrett WE Jr. Thermal effects on skeletal muscle tension behavior. Am J Sport Med 1993; 21: 517-522.

[17] Morrow DA, Haut Donahue TL, Odegard GM and Kaufman KR. Transversely isotropic tension material properties of skeletal muscle tissue. J Mech Behav Biomed 2010; 3: 124-129.

[18] Fung YC. Biomechanics: mechanical properties of living tissues. New York: Springer; 1993.

[19] Yoo L, Gupta V, Lee C, Kavehpore P and Demer JL. Viscoelastic properties of bovine orbital connective tissue and fat: constitutive models. Biomech Model Mechanobiol 2011; 10: 901-914.

[20] Burrowes KS, Iravani A and Kang W. Integrated lung tissue mechanics one piece at a time: computational modeling across the scales of biology. Clin Biomech (Bristol, Avon) 2019; 66: 20-31.

[21] Nakamura T, Takagi S, Kamon T, Yamasaki KI and Fujisato T. Development and evaluation of a removable tissue-engineered muscle with artificial tendons. J Biosci Bioeng 2017; 123: 265-271.

[22] Ehret AE, Bol M and Itskov M. A continuum constitutive model for the active behaviour of skeletal muscle. J Mech Phys Solids 2011; 59: 625-636.

[23] Teresi L and Curatolo M. Modeling and simulation of fish swimming with active muscles. J Theor Biol 2016; 409: 18-26.

[24] Tang H, Buehler MJ and Moran B. A constitutive model of soft tissue: from nanoscale collagen to tissue continuum. Ann Biomed Eng 2009; 37: 1117-1130.

[25] Gerard JM, Ohayon J, Luboz V, Perrier P and Payan Y. Nonlinear elastic properties of the lingual and facial tissues assessed by indentation technique. Application to the biomechanics of speech production. Med Eng Phys 2005; 27: 884-892.

[26] Pelteret JP and Reddy BD. Computational model of soft tissues in the human upper airway. Int J Numer Method Biomed Eng 2012; 28: 111-132.

[27] Wang YK, Nash MP, Pullan AJ, Kieser JA and Röhrle O. Model-based identification of motion sensor placement for tracking retraction and elongation of the tongue. Biomech Model Mechanobiol 2013; 12: 383-399.

[28] Cheng S, Gandevia SC, Green M, Sinkus R and Bilston LE. Viscoelastic properties of the tongue and soft palate using MR elastography. J Biomech 2011; 44: 450-454.

[29] Weickenmeier J, Itskov M, Mazza E and Jabareen M. A physically motivated constitutive model for 3D numerical simulation of skeletal muscles. Int J Numer Method Biomed Eng 2014; 30: 545-562.

[30] Bol M, Leichsenring K, Ernst M and Ehret AE. Long-term mechanical behaviour of skeletal muscle tissue in semi-confined compression experiments. J Mech Behav Biomed Mater 2016; 63: 115-124.

[31] Wang DY, He CB, Wu CQ and Zhang YS. Mechanical behaviors of tension and relaxation of tongue and soft palate: experimental and analytical modeling. J Theor Biol 2018; 459: 142-153.

[32] Kokate JY, Leland KJ, Held AM, Hansen GL, Kveen GL, Johnson BA, Wilke MS, Sparrow EM and Iaizzo PA. Temperature-modulated pressure ulcers; a porcine model. Arch Phys Med Rehabil 1995; 76: 666-673.

[33] Soares RM and Goncalves PB. Large-amplitude nonlinear vibrations of a Mooney-Rivlin rectangular membrane. J Sound Vib 2014; 333: 2920-2935.

[34] Saeidirad MH, Rohani A and Zarifneshat S. Predictions of viscoelastic behavior of pomegranate using artificial neural network and Maxwell model. Comput Electron Agric 2013; 98: 1-7.

[35] Soares RM and Goncalves PB. Nonlinear vibration and instabilities of a stretched hyperelastic annular membrane. Int J Solids Struct 2012; 49: 514-526.

[36] Yan YM. Study on hyperelastic constitutive model of rubber materials under low temperature environment. Yanshan University, China: Master's Dissertation; 2016.

[37] Jalocha D, Constantinescu A and Neviere R. Revisiting the identification of generalized Maxwell models from experimental results. Int J Solids Struct 2015; 67-68: 169-181.

[38] Hernández B, Pena E, Pascual G, Rodriguez M, Calvo B, Doblaré M and Bellón JM. Mechanical and histological characterization of the abdominal muscle. A previous step to modelling hernia surgery. J Mech Behav Biomed Mater 2011: 392-404.

[39] Takaza M, Moerman KM, Gindre J, Lyons G and Simms CK. The anisotropic mechanical behaviour of passive skeletal muscle tissue subjected to large tension strain. J Mech Behav Biomed Mater 2013; 17: 209-220.

[40] Xi M, Yun GH and Narsu B. A mathematical model on stress-strain of the epimysium of skeletal muscles. J Theor Biol 2015; 365: 175-180.

[41] Calvo B, Ramirez A, Alonso A, Grasa J, Soteras F, Osta R and Munoz MJ. Passive nonlinear elastic behaviour of skeletal muscle: Experimental results and model formulation. J Biomech 2010; 43: 318-325.

[42] Palevski A, Glaich I, Portnoy S, Eran LG and Gefen A. Stress relaxation of porcine gluteus muscle subjected to sudden transverse deformation as related to pressure sore modeling. J Biomech Eng 2006; 128: 782-787.

[43] Holzapfel GA, Gasser CT, Sommer G and Regitnig P. Determination of the layer-specific mechanical properties of human coronary arteries with non-atherosclerotic intimal thickening, and related constitutive modelling. Am J Physiol Heart Circ Physiol 2005; 289: H2048-H2058.